

ESI for

A Redox-Active Inorganic Crown Ether Based on a Polyoxometalate Capsule

Nanako Tamai,^a Naoki Ogiwara,^a Eri Hayashi,^b Keigo Kamata,^b Toshiyuki Misawa,^c Takeru Ito,^c Tatsuhiro Kojima,^d Mireia Segado,^e Enric Petrus,^e Carles Bo,^{e,f} and Sayaka Uchida*^a

a. Department of Basic Science, School of Arts and Sciences, The University of Tokyo

3-8-1 Komaba, Meguro-ku, Tokyo 153-8902 (Japan), E-mail: csayaka@g.ecc.u-tokyo.ac.jp

b. Laboratory for Materials and Structures, Institute of Innovative Research, Tokyo Institute of Technology, Nagatsuta-cho 4259, Midori-ku, Yokohama 226-8503 (Japan)

c. Department of Chemistry, School of Science, Tokai University, 4-1-1 Kitakaname, Hiratsuka 259-1292 (Japan)

d. Department of Chemistry, Graduate School of Science, Osaka University, 1-1 Machikaneyamacho, Toyonaka, Osaka 560-0043 (Japan)

e. Institute of Chemical Research of Catalonia (ICIQ), The Barcelona Institute of Science and Technology (BIST), Av. Països Catalans, 16, 43007 Tarragona (Spain)

f. Departament de Química Física i Inorgànica, Universitat Rovira i Virgili, Marcel·lí Domingo s/n, 43007 Tarragona (Spain)

Table of Contents

Title	Pages
Experimental Procedures	3–5
Table S1. Diffusion coefficients (<i>D</i>) of Cs ⁺ ion adsorption by various compounds.	6
Table S2. Langmuir parameters of Cs ⁺ ion adsorption by various compounds.	6
Table S3. Crystallographic data of I-red-Cs⁺ .	6
Fig. S1. IR spectra.	7
Fig. S2. PXRD patterns.	7
Fig. S3. Competitive adsorption of alkali metal ions.	8
Fig. S4. Wide-scan XPS spectra.	8
Fig. S5. Narrow-scan XPS spectrum (Fe 2p region).	9
Fig. S6. Narrow-scan XPS spectra (Mo 3d region).	9
Fig. S7. TDOS and PDOS at the fully oxidized (0e ⁻) state.	10
Fig. S8. Number of electrons assigned to each moiety obtained by integration of the spin density.	10
Fig. S9. TG-DTA.	11
Fig. S10. Coordination environments and bond lengths.	12
Fig. S11. Time course of oxidation-induced release of Cs ⁺ ion.	12
Fig. S12. Schematic illustration of the oxidation-induced release of Cs ⁺ ion.	13
References	14

Experimental Procedures

Materials. $\text{H}_3\text{PMo}^{\text{VI}}_{12}\text{O}_{40}\cdot n\text{H}_2\text{O}$ was purchased from Kanto Chemical Co. Inc. and used as received. $\text{FeCl}_3\cdot 6\text{H}_2\text{O}$, CH_3COOH , NaOH , ascorbic acid, aqueous chlorine solution (0.3%), CsCl , RbCl , KCl , NaCl , and distilled water were purchased from Kanto Chemical Co. Inc. and used as received. $[\alpha\text{-PMo}^{\text{VI}}_{12}\text{O}_{40}]^{3-}\text{C}[\text{Mo}^{\text{VI}}_{72}\text{Fe}^{\text{III}}_{30}\text{O}_{252}(\text{H}_2\text{O})_{102}(\text{CH}_3\text{CO}_2)_{15}]^{3+}\cdot 60\text{H}_2\text{O}$ [**I**] was synthesized according to the literature¹ as follows. $\text{H}_3\text{PMo}_{12}\text{O}_{40}\cdot n\text{H}_2\text{O}$ (4.0 g, 2.2 mmol) was dissolved in water (60 mL) and acetic acid (15 mL) was added (solution A). FeCl_3 (2.5 g, 9.2 mmol) was dissolved in 1 mol L⁻¹ NaOH (20 mL) (solution B). Solution A and B were combined and stirred until a precipitate formed. The precipitate was removed by filtration, and the resulting brown solution was allowed to stand at room temperature for one week. The resulting crystals were collected by filtration and washed with distilled water.

Syntheses. Reduction-induced uptake of Cs^+ ion was carried out as follows. Ascorbic acid (2 mg, 1.1×10^{-5} mol) was added to 0.5 mL of aqueous solution of CsCl (4 mg, 2.4×10^{-5} mol) and **I** (10 mg, 5.5×10^{-7} mol), and the aqueous solution was kept at 298 K for more than 3 h. The pH of the mixture was approximately 3. The color of the crystals turned from yellow to blue, suggesting that Mo(VI) is reduced to Mo(V) . AAS and XPS suggested the uptake of ten Cs^+ ions and electrons, and the results were fairly reproducible among the same and different batches (see below for a detailed explanation). TG shows that the reduced compound possesses approximately $49\text{H}_2\text{O}$ per chemical formula as water of crystallization, and that the molecular structure decomposes around 543 K. The reduced compound is formulated as $[\alpha\text{-PMo}^{\text{V}}_2\text{Mo}^{\text{VI}}_{10}\text{O}_{40}]^{5-}\text{C}\text{Cs}_{10}[\text{Mo}^{\text{V}}_8\text{Mo}^{\text{VI}}_{64}\text{Fe}^{\text{III}}_{30}\text{O}_{252}(\text{H}_2\text{O})_{102}(\text{CH}_3\text{CO}_2)_{15}]^{5+}\cdot 49\text{H}_2\text{O}$ [**I-red-Cs⁺**] (red stands for reduction). IR (KBr pellet) (cm^{-1}): 1620 $\delta(\text{H}_2\text{O})$, 1536 $\nu_{\text{as}}(\text{CO}_2)$, 1422 $\nu_{\text{s}}(\text{CO}_2)$, 1063 $\nu_{\text{as}}(\text{P-O})$, 961 $\nu(\text{Mo=O})$. Elemental analysis (wt%) calculated for **I-red-Cs⁺** ($\text{C}_{30}\text{H}_{347}\text{Cs}_{10}\text{Fe}_{30}\text{Mo}_{84}\text{O}_{473}\text{P}$): C 1.86, H 1.79, Cs 6.87, Fe 8.66, Mo 41.7, P 0.16; found C 2.06, H 1.02, Cs 7.42, Fe 7.90, Mo 41.0, P 0.17. Based on the results obtained from the elemental analysis by CHN combustion analysis (C and H), atomic absorption spectrometry (AAS) (Cs), and inductively coupled plasma optical emission spectrometry (ICP-OES) (Fe, Mo, and P), 11 Cs^+ rather than 10 Cs^+ per **I** could be a suitable estimate for **I-red-Cs⁺**. We conducted ten individual measurements to evaluate the time course of reduction-induced uptake of Cs^+ , as presented in Figure 2, through AAS of Cs. The results of these measurements ranged from 9.0 to 10.8 Cs^+ per **I**, with an average value of 10.2. In addition, more than five individual single-crystal X-ray diffraction measurements of **I-red-Cs⁺** suggested that 10 Cs^+ per **I** exist. Therefore, we adopted 10 Cs^+ per **I**, although it slightly deviates from the experimental result of elemental analysis. Oxidation of **I-red-Cs⁺** was carried out as follows. 4 mL of aqueous chlorine solution (0.3%) was added to **I-red-Cs⁺** (10 mg, 5.1×10^{-7} mol), and the aqueous solution was kept at 298 K for 1.5 h. The color of the crystals became yellowish, suggesting the partial oxidation of Mo(V) to Mo(VI) . AAS and XPS suggested the release six Cs^+ and electrons, and reproducibility was checked among same and different batches. Therefore, the compound obtained after the oxidation-induced release of Cs^+ is formulated as $[\alpha\text{-PMo}^{\text{V}}_2\text{Mo}^{\text{VI}}_{10}\text{O}_{40}]^{5-}\text{C}\text{Cs}_4[\text{Mo}^{\text{V}}_2\text{Mo}^{\text{VI}}_{70}\text{Fe}^{\text{III}}_{30}\text{O}_{252}(\text{H}_2\text{O})_{102}(\text{CH}_3\text{CO}_2)_{15}]^{5+}\cdot 61\text{H}_2\text{O}$ [**I-ox-Cs⁺**] (ox stands for oxidation). IR (KBr pellet) (cm^{-1}): 1618 $\delta(\text{H}_2\text{O})$, 1536 $\nu_{\text{as}}(\text{CO}_2)$, 1422 $\nu_{\text{s}}(\text{CO}_2)$, 1063 $\nu_{\text{as}}(\text{P-O})$, 961 $\nu(\text{Mo=O})$. Elemental analysis (wt%) calculated for **I-ox-Cs⁺** ($\text{C}_{30}\text{H}_{371}\text{Cs}_4\text{Fe}_{30}\text{Mo}_{84}\text{O}_{485}\text{P}$): C 1.92, H 1.97, Cs 2.83, Fe 8.93, Mo 43.0, P 0.17; found C 1.93, H 1.23 Cs 2.99, Fe 7.87, Mo 45.7, P 0.17. Notably, experimental elemental analysis data of Fe and Mo are smaller and larger, respectively, than the calculated data. Such discrepancies have been reported for **I** and related compounds,²⁻⁴ and maybe due to partial substitution of Fe with Mo (or W).

Single-crystal X-ray diffraction (SXRD) and structure analysis. X-ray diffraction data were collected at 100 K with a Rayonix-MX225-HS 2D CCD area detector by using synchrotron radiation ($\lambda = 0.61000 \text{ \AA}$) at 2D beamline of the Pohang Accelerator Laboratory (PAL), Republic of Korea. Processing of diffraction images and absorption correction were performed with HKL3000 program package.⁵ X-ray diffraction data of **I-red-Cs⁺** were additionally collected at 100 K by using synchrotron radiation ($\lambda = 0.4132 \text{ \AA}$) at BL02B1 of Spring-8, Japan. Processing of diffraction images and absorption correction were performed with the RAPID-AUTO program (Rigaku). The structure was solved by intrinsic phase method (SHELXT)⁶ and refined by the full-matrix least-squares method on F^2 using SHELXL-2018/3 crystallographic software package⁷ through Olex2⁸. In the refinement procedure, molybdenum, iron, oxygen, and cesium atoms of the POM capsule were refined anisotropically. Phosphorous atom of the encapsulated Keggin anion was assigned with a site occupancy of 1.0 and refined anisotropically. The PART and FVAR instructions of SHELXL were used to find the positions of the disordered Mo atoms. Oxygen atoms of the encapsulated Keggin anion, bridging acetates of the POM capsule, and hydrogen atoms were not included in the calculation. See Table S3 and CSD-1981851 for the crystallographic data. X-ray diffraction data of **I-ox-Cs⁺** was collected and analyzed in the same way as that of **I-red-Cs⁺**. However, the crystallinity of **I-ox-Cs⁺** is much lower than that of **I-red-Cs⁺**, because single crystals of **I-ox-Cs⁺** are prepared by treating single crystals of **I-red-Cs⁺** with aqueous chlorine solution. Crystal data for **I-ox-Cs⁺**: $\text{Cs}_4\text{Fe}_{30}\text{Mo}_{77}\text{O}_{390}\text{P}$, orthorhombic $Cmce$ (No. 64), $a = 36.468(2)$, $b = 34.928(3)$, $c = 34.810(3)$, $V = 44339(6)$, $Z = 4$, $R_1 = 0.2255$, $wR_2 = 0.5773$, $\text{GOF} = 2.341$. The crystal structures of **I-red-Cs⁺** and **I-ox-Cs⁺** are basically isostructural while the a and b -axes have been switched between the two structures.

Measurements. Combustion analysis (Elementar, vario MICRO cube) was used for the quantitative analysis of C, H, and N. Inductively coupled plasma optical emission spectrometry (ICP-OES) (Agilent Technologies, ICP-OES720) was used for the quantitative analysis of P, Mo, and Fe. Atomic absorption spectroscopy (AAS) analysis (Hitachi, ZA3000) was used for the quantitative analysis of Na, K, Rb, and Cs. Prior to the ICP-OES and AAS measurements, ca. 10 mg of the solid dispersed in a minimum amount of water followed by the addition of NH₃aq. (0.2 mL) and conc. HNO₃aq (2 mL) consecutively to dissolve the solid completely into water. The aqueous solution was diluted exactly to 50 mL. FT-IR spectra were measured by transmission method using a JASCO FT/IR 4100 instrument (JASCO). The pelletized samples were prepared by grinding and diluting the compounds (ca. 1 mg) with ca. 100 mg of KBr followed by compressing at 100 kgf cm⁻². Thermogravimetry-differential thermal analysis (TG-DTA) were conducted with a Thermo Plus 2 thermogravimetric analyzer (Rigaku) with α -Al₂O₃ as a reference under a dry N₂ flow (100 mL min⁻¹) in the temperature range of 293–773 K with an increasing rate of 10 K min⁻¹. The temperature was held at 303 K for 3 h before the temperature increase. Powder XRD patterns were measured with a New advance D8 X-ray diffractometer (Bruker) by using Cu K α radiation ($\lambda = 1.54056 \text{ \AA}$, 40 kV–40 mA) at 1.0 deg min⁻¹. X-ray photoelectron spectroscopy (XPS) was conducted with a ESCA-3400 HSE spectrometer (Shimadzu) equipped with a magnesium anode (Mg K α 1253.6 eV) operating at 10 kV–25 mA. The spectra were calibrated with the carbon 1s peak at 284.8 eV. XPS Peak 4.1 was employed to deconvolute the Mo 3d peaks to obtain the percentage of Mo(V) and Mo(VI) fractions in the compounds by using the Shirley-type baseline and an iterative least-squared optimization algorithm. Neither signals due to Fe(II) (2p_{3/2}, 709.4 \pm 0.3 eV) nor Cl (2p_{3/2}, 198.7 \pm 0.6 eV) were observed, showing that the oxidation state of iron remained +3 throughout the redox processes, and that the amounts of chlorine (due to metal chlorides and aqueous chlorine solution) in the compounds were negligible.

Competitive reduction-induced uptake of equimolar concentration of alkali metal ions from water. Ascorbic acid (5 mg, 2.8×10^{-5} mol) was added to 1 mL of an aqueous solution of NaCl (5.5 mg, 9.4×10^{-5} mol), KCl (7.4 mg, 9.9×10^{-5} mol), RbCl (11.3 mg, 9.4×10^{-5} mol), CsCl (14.9 mg, 8.9×10^{-5} mol) and I (30 mg, 1.7×10^{-5} mol). The aqueous solution was kept at 298 K for more than 4.5 h. The amounts of alkali metal ion uptakes [mol mol⁻¹] were confirmed by AAS, and were Na⁺ 0, K⁺ 0, Rb⁺ 1.1, and Cs⁺ 9.6.

Time courses and equilibrium amounts of Cs⁺ ion uptake. Ascorbic acid (2 mg, 1.1×10^{-5} mol) was added to 0.5 mL of aqueous solution of CsCl (4 mg, 2.4×10^{-5} mol) and I (10 mg, 5.5×10^{-7} mol). The solid was collected from the solution after a scheduled period and completely dissolved into water as indicated in the measurements section. The amount of Cs was quantified by AAS. Time courses of Cs⁺ ion uptake was well reproduced by the Fick's equation in radial direction.⁹

$$\frac{\partial u}{\partial t} = D \frac{\partial^2 u}{\partial r^2} \quad (1),$$

$$\frac{M_t}{M_\infty} = 1 - \frac{6}{\pi^2} \sum_{n=1}^{\infty} \frac{1}{n^2} \exp\left(-\frac{Dn^2\pi^2 t}{a^2}\right) \quad (2),$$

where, $u = cr$ (c and r are the concentration and radial coordinate, respectively), D is the diffusion coefficient, a is the particle radius, and M_t and M_∞ are the amounts of uptake at time t and equilibrium, respectively. Average particle radius was estimated as 10 μm from scanning electron microscopy (SEM) images.

Equilibrium amounts of Cs⁺ ion uptake from aqueous solutions were analyzed to illustrate the adsorption isotherm. The data could be analyzed with the commonly used Langmuir model, which is based on monolayer coverage with no interaction between the adsorbates, and can be expressed with the following equation:¹⁰

$$\frac{c_e}{q_e} = \frac{1}{K_L q_m} + \frac{c_e}{q_m} \quad (3),$$

where q_e [mg g⁻¹] and q_m [mg g⁻¹] are Cs⁺ ion adsorption capacities at equilibrium and maximum, respectively, c_e [mg L⁻¹] is the Cs⁺ ion concentration at equilibrium and K_L [L mg⁻¹] is the equilibrium constant. A plot of c_e/q_e versus c_e results in a regression line with a slope of $1/q_m$ and intercept of $1/(q_e K_L)$.

Computational Details. Electronic structure calculations at unrestricted DFT level were carried out by using the Amsterdam Density Functional program package ADF 2019v3.¹¹ The GGA functional used was the combination of OPTX¹² exchange functional and the PBE¹³ correlation correction, also known as OPBE.¹⁴ We included the scalar Zero Order Relativistic Approach ZORA^{15,16} together with the standard TZP basis set, frozen core treatment, and default numerical integration scheme. Solvent effects were introduced making use of the continuous solvent model COSMO with default parameters for water.¹⁷ A data set collection of computational results is available in the ioChem-BD repository¹⁸ and can be accessed online following the link <https://doi.org/10.19061/iochem-bd-1-162>. Given the size and complexity of the POM capsule I, we needed to define a computationally amenable model. The system consists of two parts: the external capsule and the inner Keggin anion. For the external capsule, we considered the spherical cluster [Mo^{VI}₇₂Fe^{III}₃₀O₂₅₂(H₂O)₆₀]¹⁸⁺ [I-capsule], which lacks the internal acetate ligands but keeps icosahedral symmetry (I_h) and octahedral Fe(III) ions. Considering the fifteen

internal acetate ligands disordered among 30 iron centers is an effort out of reach. Our previous work on Keplerates showed that the nature of the internal capsule decoration does not affect the main electronic properties of these compounds.¹⁹ Hence, we did not take into account the acetate ligands nor any additional encapsulated solvent molecules, just only two water molecules per iron center were explicitly included so to keep octahedral coordination. The internal Keggin anion [α -PMo^{VI}₁₂O₄₀]³⁻ [**I-Keggin**], was considered as it is without any further simplification. Firstly, we independently optimized the geometries of **I-Keggin** and **I-capsule** under their own symmetry constraints. **I-capsule** achieved self-consistency and converged to a high-spin solution with the 150 unpaired electrons in accordance to the formal Fe(III) oxidation state. Then, the whole system [α -PMo^{VI}₁₂O₄₀⊂Mo^{VI}₇₂Fe^{III}₃₀O₂₅₂(H₂O)₆₀]¹⁵⁺ [**I-all**] was considered, thus the union of **I-Keggin** and **I-capsule** while retaining C₂ symmetry. We followed the same scheme for the reduced capsules with 1, 6, 12, 18 and 24 additional electrons. Other intermediate reduction states were found electronically unstable, i.e., it was not possible to find a self-consistent solution because of spatial localization and accidental degeneracy of the energy levels, which is reminiscent of the higher symmetry of the fragments.

Table S1. Diffusion coefficients (*D*) of Cs⁺ ion adsorption by various compounds

Compound	<i>D</i> [cm ² s ⁻¹]	Temp [K]	Ref
cement paste solids	8.9×10 ⁻⁷	343	1
FROCOR soil	5.9×10 ⁻⁷	298	2
Saponite clay minerals	2.5×10 ⁻⁸	423	3
Zeolite (Na-CHA)	4.0×10 ⁻⁹	298	4
I	2.4×10 ⁻⁹	298	This work
P ₂ W ₁₈ -Cr(III) complex	1.3×10 ⁻¹⁰	r.t.	5
P ₂ Mo ₁₈ -Cr(III) complex	1.0×10 ⁻¹⁰	r.t.	5
SiMo ₁₂ -Cr(III) complex	8.2×10 ⁻¹²	343	6

1. K. G. Papadokostaki and A. Savidoub, *J. Hazard. Mater.* 2009, **171**, 1024–1031. 2. D. Aldaba, A. Rigol and M. Vidal, *J. Hazard. Mater.* 2010, **181**, 1072–1079. 3. K. Fujimoto, K. Sato and M. Nakata, *J. Phys. Soc. Jpn.* 2017, **86**, 034901. 4. S. M. Robinson, W. D. Arnold and C. H. Byers, *AIChE J.* 1994, **40**, 2045–2054. 5. S. Hitose and S. Uchida, *Inorg. Chem.* 2018, **57**, 4833–4836. 6. S. Seino, R. Kawahara, Y. Ogasawara, N. Mizuno and S. Uchida, *Angew. Chem., Int. Ed.* 2016, **55**, 3987–3991.

Table S2. Langmuir parameters of Cs⁺ ion adsorption by various compounds

Compound	<i>q_m</i> [mg g ⁻¹]	<i>K_L</i> [L mg ⁻¹]	Temp [K]	Ref
PAN-KNiCF	157.73	1.46×10 ⁻¹	303	1
Ferrite	108.58	8.15×10 ⁻⁴	296	2
mesoporous hybrid adsorbent (MHA)	97.63	2.01	r.t.	3
I	87.72	1.24×10 ⁻³	298	This work
Magnetite	70.77	3.53×10 ⁻⁴	296	2
natural clinoptilolite	49.02	2.28×10 ⁻⁴	293	4
SM-AMP20	36.09	9.3×10 ⁻²	298	5

1. Z. Du, M. Jia and X. Wang, *J. Radioanal. Nucl. Chem.* 2013, **298**, 167–177. 2. R. R. Sheha and E. Metwally, *J. Hazard. Mater.* 2007, **143**, 354–361. 3. M. R. Awual, Y. Miyazaki, T. Taguchi, H. Shiwaku and T. Yaita, *Chem. Eng. J.* 2016, **291**, 128–137. 4. I. Smičiklas, S. Dimović and I. Plečaš, *Appl. Clay Sci.* 2007, **35**, 139–144. 5. H. Deng, Y. Li, Y. Huang, X. Ma, L. Wu and T. Cheng, *Chem. Eng. J.* 2016, **286**, 25–35.

Table S3. Crystallographic data of I-red-Cs⁺.

I-red-Cs ⁺	
Crystal system	orthorhombic
Space group	<i>Ccmb</i>
Unit cell	<i>a</i> = 35.0800(7) <i>b</i> = 36.9265(7) <i>c</i> = 34.8114(6)
Volume	45094.0(15)
<i>Z</i>	4
<i>D_{calc}</i> (g cm ⁻³)	2.501
<i>F</i> (000)	31716
<i>h, k, l</i> range	–45/45, –47/47, –45/44
<i>μ</i> (mm ⁻¹)	3.621
<i>R₁</i> (<i>I</i> > 2σ(<i>I</i>))	0.0701
<i>wR₂</i> (all data)	0.1940
GOF on <i>F</i> ²	1.021

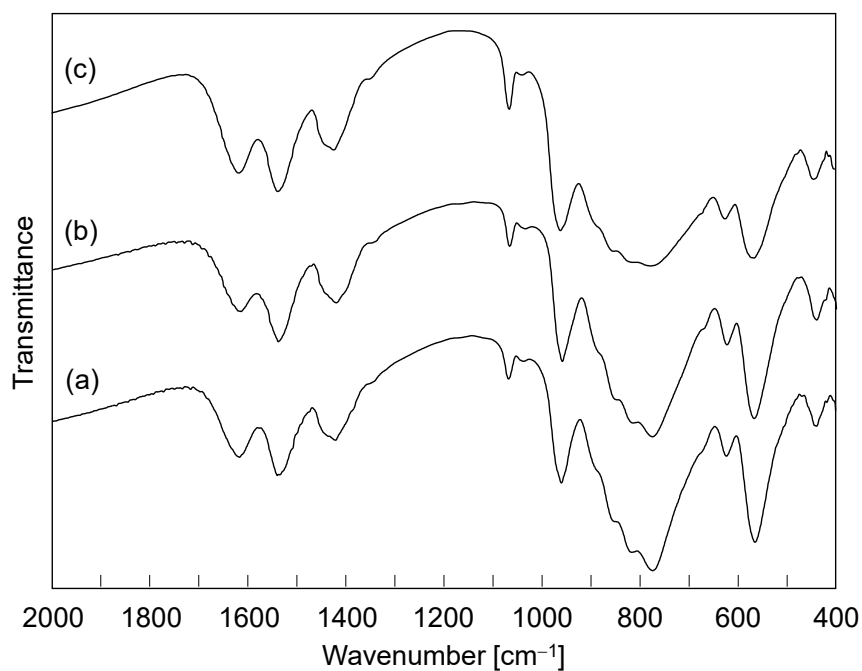


Fig. S1 IR spectra of (a) I, (b) I-red-Cs⁺, and (c) I-ox-Cs⁺.

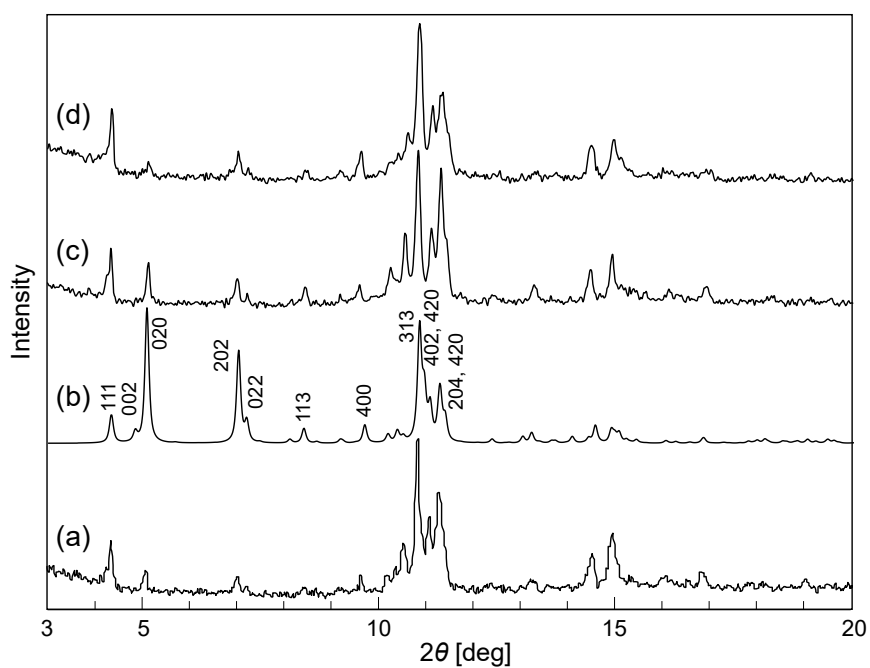


Fig. S2 PXRD patterns of (a) I, (b) I-red-Cs⁺ (calc) with Miller indices, (c) I-red-Cs⁺ (exp), and (d) I-ox-Cs⁺.

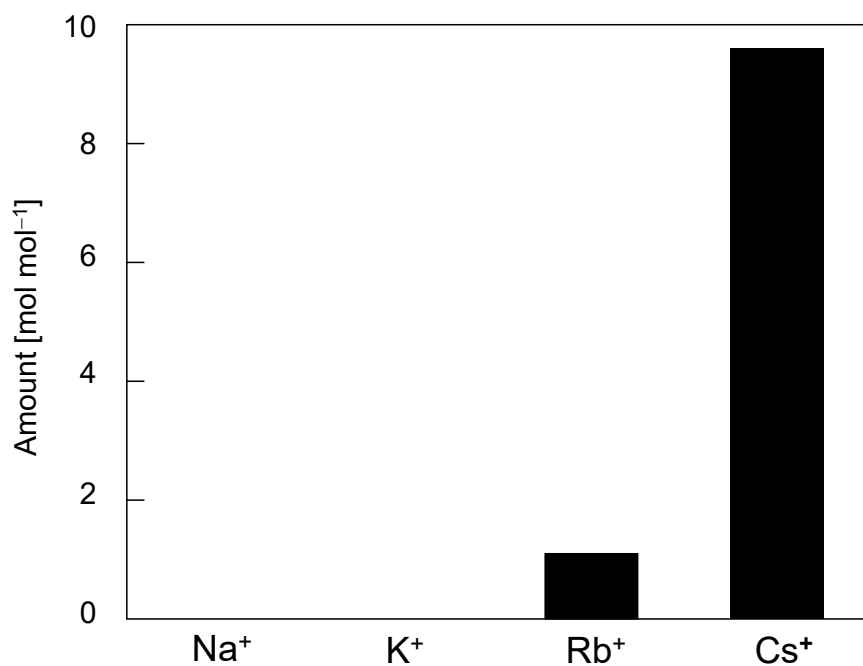


Fig. S3 Competitive adsorption of alkali metal ions by I at 298 K.

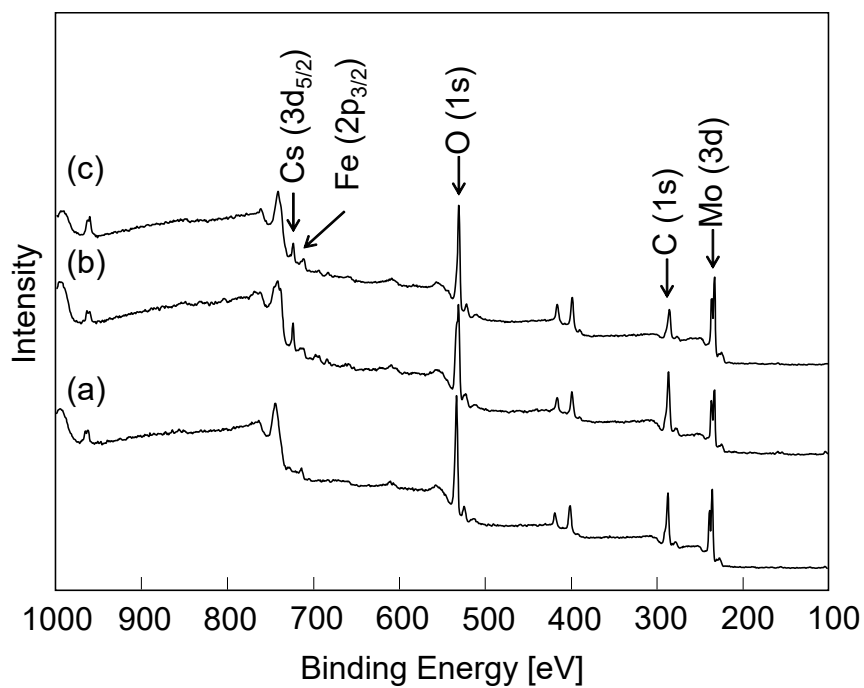


Fig. S4 Wide-scan XPS spectra of (a) I, (b) I-red-Cs⁺, and (c) I-ox-Cs⁺.

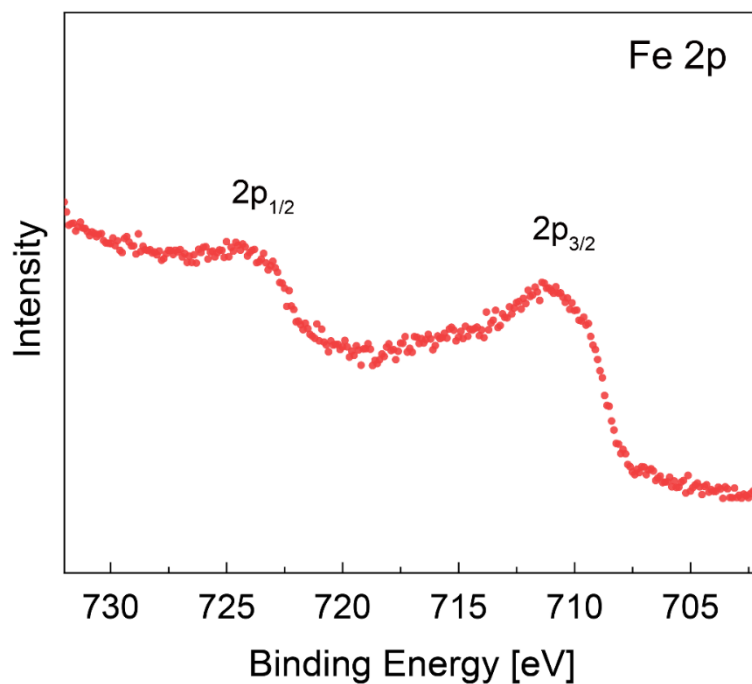


Fig. S5 Narrow-scan XPS spectrum (Fe 2p region) of **I-red-Cs***. The signals at the lower and higher energies indicate the Fe $2p_{3/2}$ and Fe $2p_{1/2}$ signals, respectively.

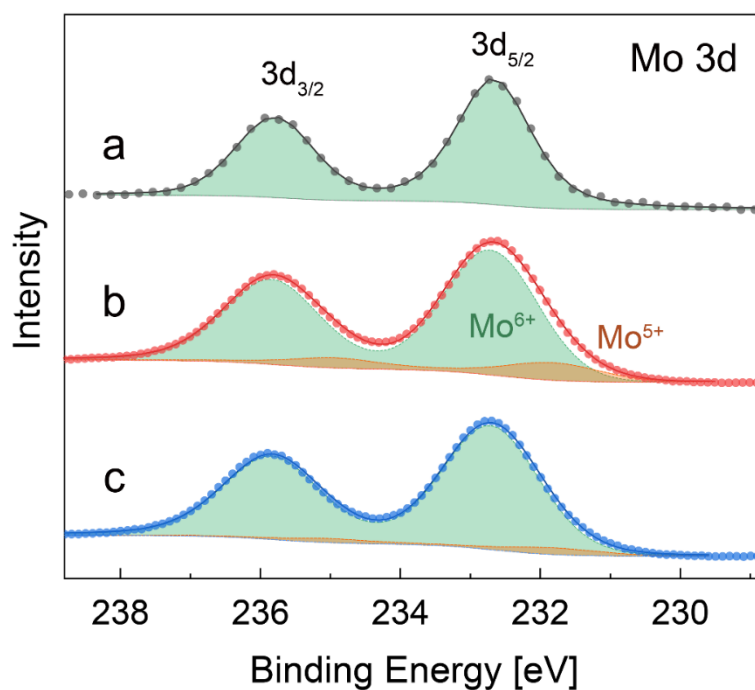


Fig. S6 Narrow-scan XPS spectra (Mo 3d region) of (a) **I**, (b) **I-red-Cs***, and (c) **I-ox-Cs***. The signals at the lower and higher energies indicate the Mo $3d_{5/2}$ and Mo $3d_{3/2}$ signals, respectively. Orange and green peaks show the Mo(V) and Mo(VI) species, respectively.

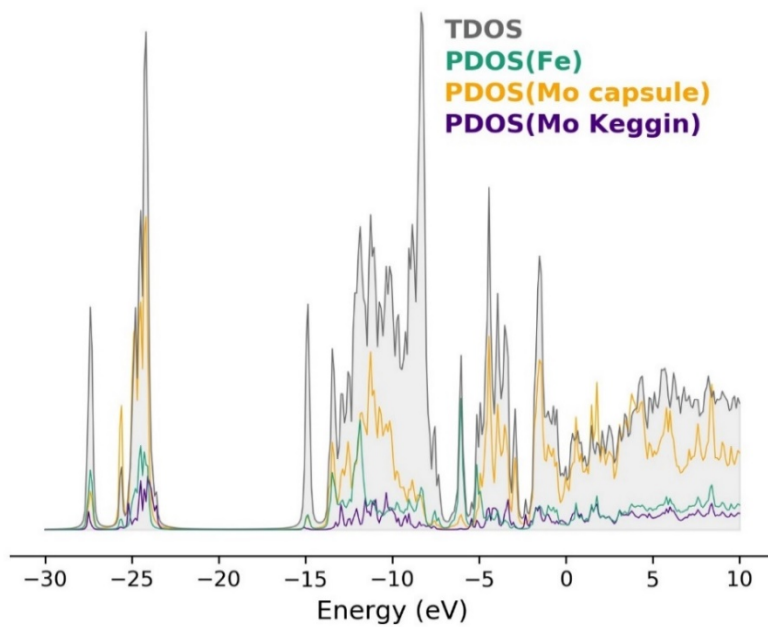


Fig. S7 TDOS (grey) and PDOS for Fe (green), Mo Keggin (internal Mo atoms, purple) and Mo capsule (external Mo atoms, yellow) for I-all at the fully oxidized ($0e^-$) state.

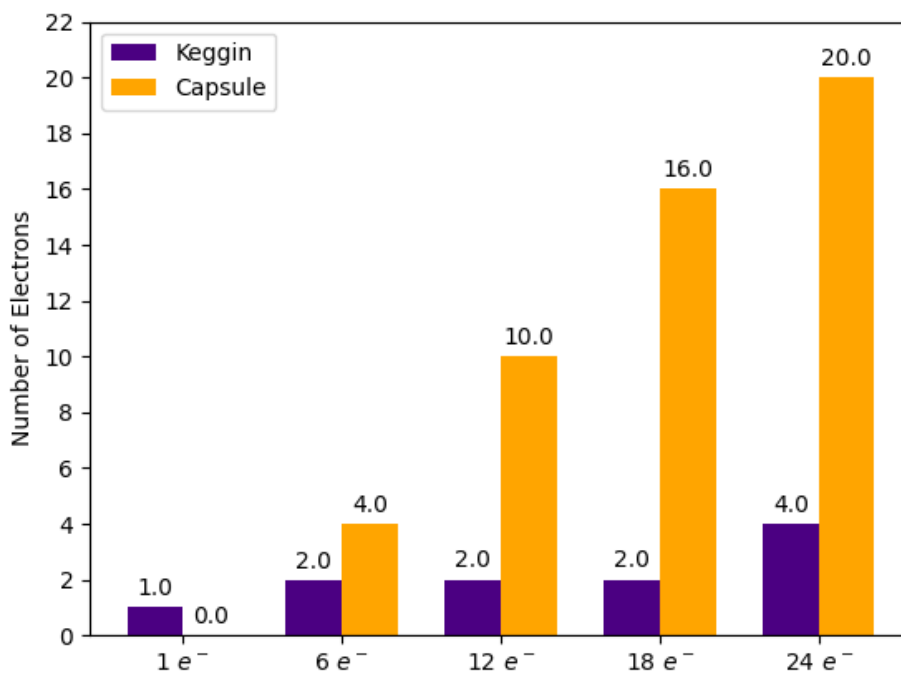


Fig. S8 Number of electrons assigned to each moiety (I-Keggin and I-capsule) in I-all obtained by integration of the spin density.

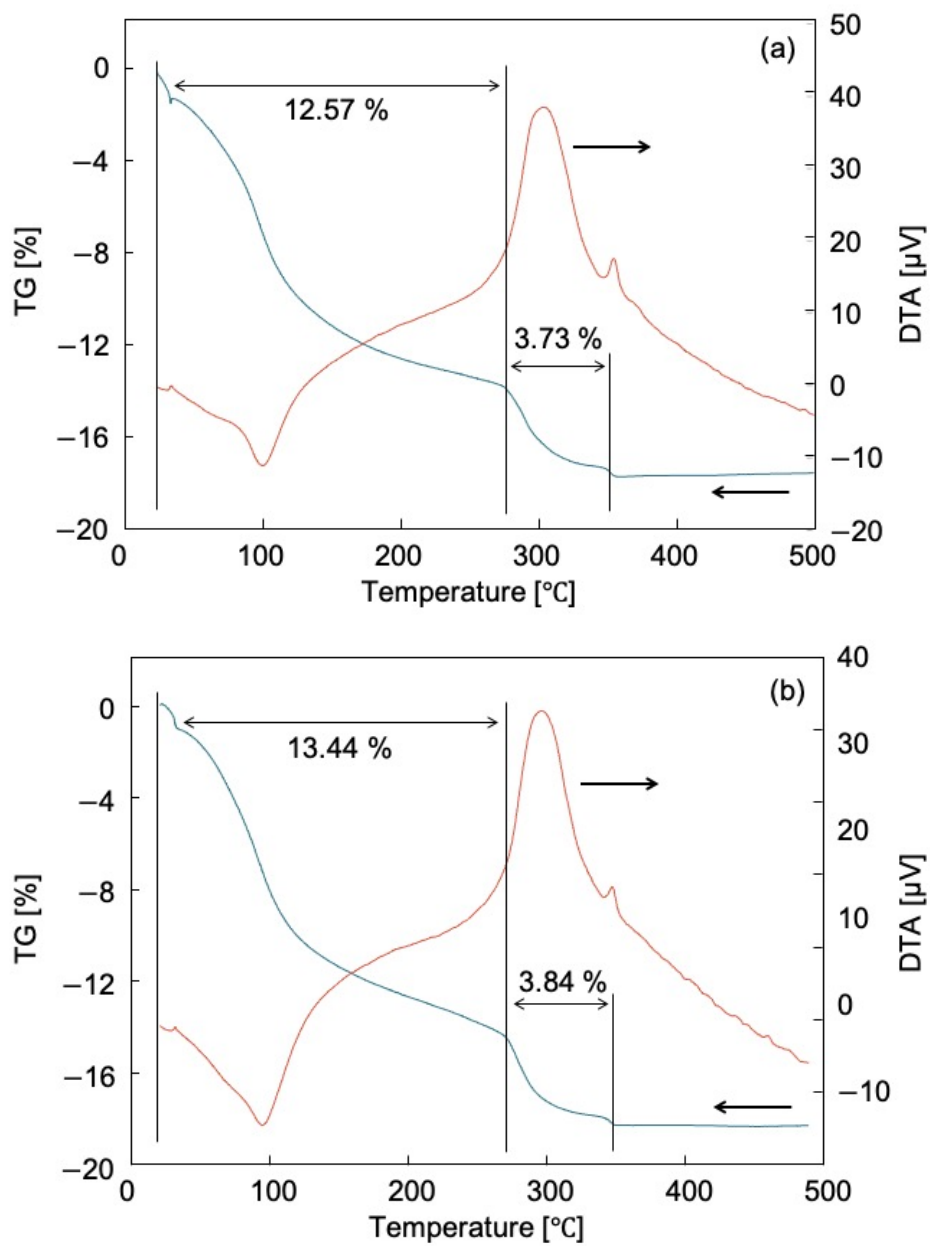


Fig. S9 TG-DTA of (a) **I-red-Cs⁺** and (b) **I-ox-Cs⁺**. The first and second weight loss correspond to the loss of water molecules and acetate ligands, respectively.

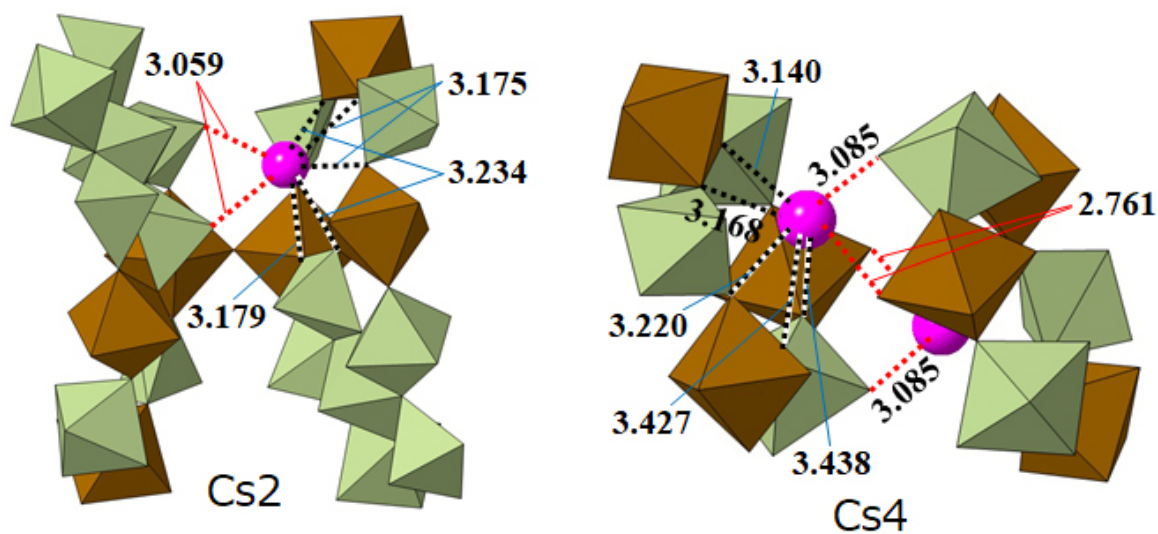


Fig. S10 Coordination environments and bond lengths of Cs2 and Cs4. Red and black broken lines show the Cs–O bonds connecting the POM capsules and coordinating to the crown-ether-like pores of $\{Mo_3Fe_3O_6\}$.

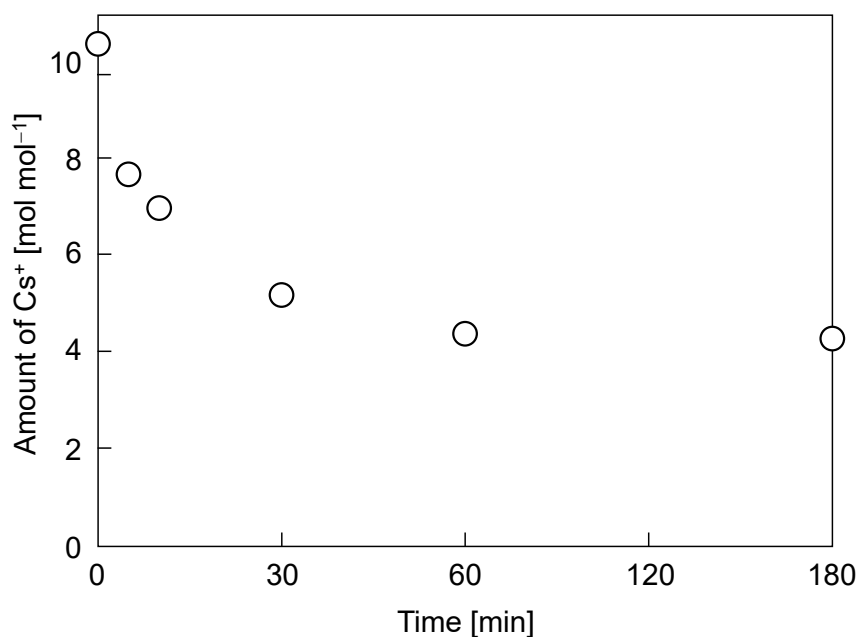


Fig. S11 Time course of oxidation-induced release of Cs⁺ ion from I-red-Cs⁺ at 298 K.

The result suggests that I-red-Cs⁺ is not fully oxidized and weakly reduced after the oxidation-induced release of Cs⁺ ion. To gain further insight, redox titration was conducted to estimate the amount of transferred electric charge (i.e., degree of electron transfer) in the redox process by the following method: I (40 mg) was mixed with carbon paste (60 mg) and a modified electrode was obtained. Then, the i (current) $-t$ (time) curve was obtained by the amperometry technique by using the modified electrode as a working electrode in 0.1 mol L⁻¹ Na₂SO₄ electrolyte (pH = 5.6), graphite counter electrode, and Ag/AgCl (+0.201 V vs. NHE) reference electrode. Ascorbic acid and CsCl were added, allowed to reach equilibrium, followed by the addition of chlorine water. The time course showed that the amounts of transferred electric charges in the reduction-induced Cs⁺ ion uptake and oxidation-induced Cs⁺ release processes are 11.3 [C] and 6.6 [C], respectively. These findings indicate that the degree of electron transfer in the oxidation process is about 60% of that in the reduction process, which is consistent with the amounts of adsorption and desorption of Cs⁺ ions (Figs. 2 and S11).

Fig. S12 Schematic illustration of the oxidation-induced release of Cs⁺ ion from **I-red-Cs⁺** to form **I-ox-Cs⁺**. Green and brown polyhedra show the [MoO₆] and [FeO₆] units, respectively. Blue and pink spheres show the Cs captured in the crown-ether-like pores of {Mo₃Fe₃O₆} and those connecting adjacent POM capsules, respectively. Red circles indicate the Cs connecting adjacent POM capsules. Local structures of Cs (Cs2 and Cs3) connecting adjacent POM capsules are shown in the red rectangles. The crystal structures of **I-red-Cs⁺** and **I-ox-Cs⁺** are basically isostructural while the *a* and *b*-axes have been switched between the two structures. The crystal structure (the axes) of **I-ox-Cs⁺** is depicted according to that of **I-red-Cs⁺**.

References

1. A. Müller, S. K. Das, H. Bögge, M. Schmidtman, A. Botar and A. Patrut, *Chem. Commun.* 2001, 657–658.
2. H. Taghiyar and B. Yadollahi, *Polyhedron* 2018, **156**, 98–104.
3. A. M. Todea, J. Szakacs, S. Konar, H. Bögge, D. C. Crans, T. Glaser, H. Rousseliere, R. Thouvenot, P. Gouzerh and A. Müller, *Chem. Eur. J.* 2011, **17**, 6635–6642.
4. A. M. Todea, A. Merca, H. Bögge, T. Glaser, J. M. Pigga, M. L. K. Langston, T. Liu, R. Prozorov, M. Luban, C. Schröder, W. H. Casey and A. Müller, *Angew. Chem., Int. Ed.* 2010, **49**, 514–519.
5. W. Minor, M. Cymborowski, Z. Otwinowski and M. Chruszcz, *Acta Cryst. D* 2006, **62**, 859–66.
6. G. M. Sheldrick, *Acta Crystallogr., Sect. A: Found. Adv.*, 2015, **71**, 3–8.
7. G. M. Sheldrick, *Acta Crystallogr., Sect. C: Struct. Chem.*, 2015, **71**, 3–8.
8. O. V. Dolomanov, L. J. Bourhis, R. J. Gildea, J. A. K. Howard and H. Puschmann, *J. Appl. Crystallogr.*, 2009, **42**, 339–341.
9. J. Crank, *The Mathematics of Diffusion*. Oxford University Press, London, Chapter 6, 1956.
10. P. Atkins and J. de Paula, *Physical Chemistry 8th edition*, Oxford University Press, London, Chapter 25, 2006.
11. a. SCM, Theoretical Chemistry, Vrije Universiteit, Amsterdam, The Netherlands, <http://www.scm.com>). B. G. te Velde, F. M. Bickelhaupt, E. J. Baerends, C. F. Guerra, S. J. A. van Gisbergen, J. G. Snijders and T. Ziegler, *J. Comput. Chem.* 2001, **22**, 931–967.
12. W. M. Hoe, A. J. Cohen and N. C. Handy, *Chem. Phys. Lett.* 2001, **341**, 319–328.
13. A. D. Becke, *Phys. Rev. A* 1988, **38**, 3098–3100.
14. M. Swart, A. W. Ehlers and K. Lammertsma, *Mol. Phys.* 2004, **102**, 2467–2474.
15. E. van Lenthe, E. J. Baerends, J. G. Snijders, *J. Chem. Phys.* 1993, **99**, 4597–4610.
16. E. Van Lenthe and E. J. Baerends, *J. Comput. Chem.* 2003, **24**, 1142–1156
17. A. Klamt, *J. Phys. Chem.* 1995, **99**, 2224–2235.
18. M. Álvarez-Moreno, C. de Graaf, N. López, F. Maseras, J. M. Poblet and C. Bo, *J. Chem. Inf. Model.* 2015, **55**, 95–103.
19. D. Melgar, N. A. G. Bandeira and C. Bo, *Chem. Eur. J.* 2017, **23**, 5338–5344.